Molecular dynamics of NaCl (B1 and B2) and MgO (B1) melting: Two-phase simulation

Anatoly B. Belonoshko and Leonid S. Dubrovinsky

Theoretical Geochemistry Program, Institute of Earth Sciences, Uppsala University, Uppsala S-752 36, Sweden

Abstract

Melting of NaCl and MgO has been simulated with a two-phase molecular dynamics method at constant pressure using newly developed interaction potentials. Equations of state for NaCl and MgO simulated by molecular dynamics are in good agreement with available experimental data. Equations of state for MgO and NaCl were obtained by fitting simulated volumetric properties at pressures and temperatures up to 300 kbar and 3000 K (for NaCl) and 2000 kbar and 7000 K (for MgO). The pressure dependence of the melting temperature was predicted up to 1000 and 1400 kbar for NaCl and MgO, respectively. Crystallization and melting were observed without hysteresis. The simulated melting curve of NaCl is fully consistent with experimental measurements. The pressure dependence of the melting temperature of MgO is consistent with experimental data at 1 bar and previous theoretical estimations by Jackson (1977) and Ohtani (1983). The melting temperature of MgO is substantially higher than that determined by Zerr and Boehler (1994) (by 1000 K at 300 kbar) and substantially lower than that predicted by Cohen and Gong (1994) (by 1500 K at 300 kbar). The melting temperature of MgO at the pressure of the core-mantle boundary is calculated to be 6900 ± 200 K. The procedures for simulation of melting of NaCl and MgO, starting from a calculation of the interatomic potential and ending with analysis of results, are identical.

Introduction

Melting is probably the most familiar first-order transition. Surprisingly, despite significant efforts, relatively little is known about its nature. Thus, until now, the prediction of the pressure dependence of the melting temperature (T_m) of a solid has been problematic. This dependence, however, is very important for a description of Earth's evolution, especially if we adopt the hypothesis of an early magma ocean (Agee and Longhi 1992; Agee 1993; Anderson 1989). Pressure dependence of the melting temperature of minerals forming the Earth's mantle is necessary to describe the timing and sequence of crystallization from the protomelt (Solomatov and Stevenson 1993). Because MgO is believed to be one of the major constituents of the Earth's mantle (Anderson 1989), the attention that MgO receives [e.g., Zerr and Boehler (1994) and references therein] is quite understandable.

There has been significant progress lately in the experimental determination of the pressure (P) dependence of the melting temperature (T) of iron, $MgSiO_3$ perovskite, stishovite, and wüstite (Boehler 1992, 1993; Heinz and Jeanloz 1987; Knittle and Jeanloz 1991; Saxena et al. 1993; Shen et al. 1993; Shen 1994; Yoo et al. 1993; Zerr and Boehler 1993b) under the physical conditions of the Earth's mantle and core using a diamond-anvil cell with laser heating and shockwave techniques. Zerr and Boehler (1994) recently measured the melting temperature of MgO up to 315 kbar. However, some of the experiments have yielded quite controversial results. Experimentally

determined melting temperatures of iron, FeO, and $MgSiO_3$ perovskite differ by up to thousands of degrees. In such situations, a theoretical approach can provide independent information to support experimental determinations.

Until recently, the differences in theoretical predictions of the melting curve for $MgSiO_3$ perovskite (Matsui and Price 1991; Kapusta and Guillopé 1993; Kubicki and Lasaga 1992) were even greater than the differences in the experimental measurements (disagreement by about 2500 K). Recently, Belonoshko (1994) used a two-phase molecular dynamics (MD) simulation at constant pressure with an interatomic potential (IP) developed by Matsui and Price (1991) to describe the melting P-T curve of $MgSiO_3$ perovskite and explained the reasons for such differences. There was almost perfect agreement between the MD simulation and experiment of Zerr and Boehler (1993a, 1993b). We do not see any reason why the simulation should be incorrect, because the Matsui-Price IP reproduces all structural modifications of $MgSiO_3$ and, therefore, should be suitable for the modeling of phases with different coordination, and hence for the simulation of liquid $MgSiO_3$. The simulated PVT properties of $MgSiO_3$ are also in good agreement with experimental data. Because the melting T at a given P is one of several energetic properties, one would expect that this particular property could be calculated with about the same precision as the others. Still, mindful of the controversy between various experimental determinations of the perovskite melting curve, we decided to simulate the melting

curve of NaCl (B1 and B2), which, unlike the melting curve of MgSiO₃ perovskite, is well determined (Akella et al. 1969). Because NaCl is probably the most extensively studied compound, both experimentally (Akella et al. 1969; Birch 1986; Boehler and Kennedy 1980; Heinz and Jeanloz 1984; Liu and Bassett 1973; Sato-Sorensen 1983) and theoretically (Dekker 1965; Dove 1993; Hemley and Gordon 1985; Jha 1993), we are able to compare our results with previous work. After successfully simulating the NaCl (B1) melting curve (this study), with full agreement with experimental results, we studied MgO by the same method of two-phase MD simulation at constant pressure.

The paper is organized as follows. First, we describe the method and interatomic potentials used. Next, the simulated thermoelastic properties and melting *P-T* curves of NaCl and MgO are compared with the available experimental and previously calculated data. Finally, we summarize our results. The influence of system size on calculated results is discussed in the Appendix.

DESCRIPTION OF THE METHOD

Molecular dynamics simulation is a well-established technique in mineralogy, especially for studying the effects of high pressure and temperature on the properties of solids and their melts. Detailed descriptions of the method are given in many textbooks (e.g., Allen and Tildesley 1987; Haile 1992). Briefly, MD solves Newton's equations of motion for atoms placed in a so-called computational box. Forces are calculated with given interatomic potentials. The procedure becomes somewhat more complicated if constant pressure is required, but the main features remain essentially the same.

MD simulation in its classical modification (periodic boundary conditions and *NVE* ensemble, where N = number of atoms, V = volume, and E = energy) is quite suitable for calculation of thermoelastic properties of a solid or a melt. However, simulation of a melting transition is complicated. Overheating of a crystal in MD simulation of melting is a well-known phenomenon. For example, Matsui and Price (1991) and Kapusta and Guillopé (1993) reported that significant overheating (about 1500 K) is required for melting MgSiO₃ perovskite. Smolander (1990) noticed that copper melting in Monte Carlo simulation requires overheating by a few hundred degrees. Kubicki and Lasaga (1992) reported that overheating is required for the melting of forsterite. Overheating is required for several reasons. First, a nucleus of melt is unstable unless it reaches a certain size (Landau and Lifshitz 1958), which might be quite large compared with the size of the computational box (which usually does not exceed a few dozen angstroms). Therefore, appearance of melt is suppressed by size restrictions, and overheating is required to decrease the size of a stable nucleus. Second, the creation of an interface between solid and melt requires excess energy, which can be provided only by increasing temperature. Third, simulations at constant volume might lead to instability of both solid

and liquid phases (the volume is too small for a liquid and too large for a solid).

To solve the overheating problem, there are two possible solutions. One is to increase the size of the simulated system. This leads to a tremendous increase of computational time required for the simulation, and the results are still uncertain because systems containing as many as 100 000 atoms may not be large enough for the appearance of melt nuclei. Moreover, it is rather doubtful that melt nuclei will appear in an ideal crystal without overheating. The second solution, which we favor, is to introduce an interface as a starting configuration. In other words, place a presimulated melt and a presimulated crystal in the computational box. This approach was successfully used by Kubicki and Lasaga (1992) for simulation of forsterite melting. Belonoshko (1994) simulated MgSiO₃ perovskite melting in agreement with experimental data (Zerr and Boehler 1993a, 1993b) using this approach and the interatomic potential of Matsui and Price (1991). Note, that both Belonoshko (1994) and Matsui and Price (1991) used the same potential and simulated MgSiO₃ perovskite at constant pressure. Belonoshko (1994) did not notice any significant overheating, whereas Matsui and Price (1991) did. Phillpot et al. (1989) studied melting of Si and found that "melting in real crystals should be initiated at grain boundaries and surfaces, a conclusion that is entirely in accord with experiment." Therefore, we believe that two-phase simulation at constant pressure indeed provides a tool for studying the melting transition.

Derivation of interatomic potentials

Although several IPs are available for both NaCl (Anastasiou and Fincham 1982) and MgO (Allan et al. 1991; Cohen and Gordon 1976; Isaak et al. 1990; Matsui 1989; Leinenweber and Navrotsky 1988; Wolf and Bukowinski 1988) we calculated our potentials using identical procedures for NaCl and MgO at all stages of the work.

The procedure for the calculation of IP parameters is similar to that used in the METAPOCS computer program (Parker et al. 1984; Urusov et al. 1994). The procedure consists of minimization of the difference between experimental and calculated properties as a function of IP parameters.

Because of our interest in thermoelastic properties, we chose the goal function of the following form:

$$\sum_{i=1}^{p} (X_i - X_i^{exp})^2 + \omega_C \sum_{1}^{21} (C_{ij} - C_{ij}^{exp})^2$$

$$+ \omega_\alpha \sum_{1}^{3} (\alpha_i - \alpha_i^{exp})^2 + \omega_H (H - H^{exp}) \to \min \quad (1)$$

where X_i = structural parameters, C_{ij} = elastic constants, α_i = coefficient of linear thermal expansion, H = enthalpy, ω = weight, and exp = experimental values. The particular values of ω_C, ω_α, and ω_H were chosen so that all terms in Equation 1 have the same order of magnitude.

During the calculation procedure, the IP must correctly reproduce the symmetry of the structure and the positions of all atoms (except the one fixed at the origin), because cubic symmetry is not initially assumed (and should not be if the IP is to work properly). Hence, in our case the total number (p in Eq. 1) of variable structural parameters (lattice parameters and coordinates of independent atoms) is equal to 27 for the B1 structure.

Enthalpy, $H_{P,T}$, at given P and T was simulated using the following equation (Born and Huang 1954; Parker and Price 1989):

$$H_{P,T} = \frac{1}{2} \sum_{l,m} \phi_{lm} + \sum_i^M \left\{ \frac{\hbar\omega_i}{2} + \frac{\hbar\omega_i}{\left[1 - \exp\left(-\frac{\hbar\omega_i}{2kT}\right)\right]} \right\}$$
$$+ \sum_i^L \Delta E_i \qquad (2)$$

where ϕ_{lm} is the pair potential of interatomic interaction, k is Boltzmann's constant, $\hbar$ is Planck's constant, M is the total number of phonon frequencies, ω_i is frequency, L is the number of atoms per formula unit, and ΔE_i is the energy of the charge transfer. The physical meaning, the method of determination, and values of ΔE_i are given in Urusov (1975, chapters 1 and 4), Urusov and Dubrovinsky (1989, chapter 5), Urusov et al. (1994) [in our particular case, the calculated optimal IPs for Mg and Na with effective charges are 1.251e and 0.966e, respectively; correspondingly, $\Delta E_{Mg}(1.251) = 326.37$ kcal, $\Delta E_O(-1.251) = -43.47$ kcal, $\Delta E_{Na}(0.966) = 110.20$ kcal, and $\Delta E_{Cl}(-0.966) = -27.24$ kcal].

For every given vector of reciprocal lattice $\mathbf{q}$ within the first Brillouin zone, a set of frequencies ω_i is obtained as a result of solution of the corresponding determinant equation

$$|D(\mathbf{q}) - I\,\omega^2(\mathbf{q})| = 0 \qquad (3)$$

where $D(\mathbf{q})$ is the dynamic matrix (Born and Huang 1954) and I is the identity matrix.

Frequencies were calculated on a three-dimensional mesh of 64 points within the first Brillouin zone. Parker and Price (1989) showed that for temperatures above 50 K thermodynamic properties converge rapidly with a mesh of this size, and for the materials considered here there are only small differences in the magnitude of the thermodynamic properties for a mesh containing more than eight distinct points.

Elastic constants were calculated according to previously described methods (Catlow and Macrodt 1982; Parker and Price 1989). The thermal expansion coefficient was calculated according to Animalu (1977).

We used the nongradient Powell method (Press et al. 1992) to minimize the function on the left side of Equation 1. This method was chosen because the analytical calculation of derivatives of the goal function (Eq. 1) in its general form is difficult. On the other hand, numerical calculation of the derivatives decreases the precision of the results.

The form of the IP is as follows:

$$\phi_{ij} = q_i q_j/R_{ij} + \epsilon_{ij}\, f\,(\rho_i + \rho_j)\exp[(r_i + r_j - R_{ij})/(\rho_i + \rho_j)]$$
$$+ \sqrt{(1 - \epsilon_{ij})}\, D_{ij}\{\exp[-2\alpha_{ij}\,(R_{ij} - R_{ij0})]$$
$$- 2\exp[-\alpha_{ij}\,(R_{ij} - R_{ij0})]\} - C_{ij}/R_{ij}^6 \qquad (4)$$

where i and j = atomic indexes, q = effective charge, ρ and r = parameters of Gilbert-like repulsive potential, f = units constant (1 kcal/mol), D, α, and R_0 = parameters of the Morse potential, C = van der Waals constant, ϵ_{ij} is the bond ionicity, and $q_i q_j/z_i z_j$, z = formal charge. This form of IP was first applied by Hofer and Ferreira (1966) to describe interactions in alkali halides. Later, this IP was compared with other forms of IP (Urusov and Dubrovinsky 1985, 1989) and found to produce better fits to experimental data than the Born-Mayer and Morse potentials. Note that in the extreme cases where $\epsilon = 0$ and $\epsilon = 1$, this IP transforms into the Morse and Buckingham potentials, respectively.

Experimental data for structure, elastic constants, coefficients of thermal expansion, and enthalpy at 300 K and 1 bar were fitted with our potential. We did not calculate C_{44} because a central force IP gives the value $C_{44} = C_{12}$. The experimental and calculated data are given in Table 1. (Note that in cubic symmetry $\alpha_1 = \alpha_2 = \alpha_3 = \alpha/3$; values of elastic constants other than C_{11} and C_{12} are not listed, their values corresponding to cubic symmetry.) The calculated IP parameters are given in Table 2. Values of charges in our model are close to those calculated earlier. Charges of Na and Cl are near 1. The charge of Mg is about the same as the Mg charges of 1.37 and 1.4 calculated by Leinenweber and Navrotsky (1988) and by Matsui (1989), respectively. The O charge follows from electroneutrality.

Description of molecular dynamics simulations

We performed two kinds of MD simulations. Simulation of PVT data utilized a one-phase simulation at constant volume for which the number of particles in the computational box was 512 (256 molecules) with three-dimensional periodic boundary conditions to mimic bulk behavior. A two-phase simulation at constant pressure was used for the simulation of the melting transition. The two-phase MD simulation requires some explanation (see also Belonoshko 1994).

To determine the P-T conditions of melting in an MD simulation, it is quite natural to put liquid and solid parts together so that they have a common interface and to observe in the course of the simulation which phase grows. This is exactly what we did. The left and right parts of the computational box were filled with initial simulated melt and crystal, respectively. The number of particles in the computational box was 1024 (512 in the liquid part and 512 in the solid part). Periodic boundary conditions

TABLE 1. Comparison of calculated and experimentally measured lattice parameters, elastic moduli, coefficient of thermal expansion, and enthalpy

Obs. value	Halite		Periclase	
	Calc.	Exp.	Calc.	Exp.
a (nm)	0.5648	0.5640*	0.4212	0.4213*
C_{11} (GPa)	49.2	48.99**	304	292†
C_{12} (GPa)	15.7	12.57**	103	92†
α ($\times 10^{+5}$ K^{-1})	1.26	1.169‡	3.31	3.11§
H_t (kcal/mol)	−93.31	−92.25§	−143.4	−143.8§

* Kracek and Clark (1966).
** Bartels and Schuele (1965).
† Zoubolis and Grimsditch (1991).
‡ Boehler and Kennedy (1980).
§ Saxena et al. (1993).

were also applied to the two-phase simulation; therefore, each semi-infinite slab (either liquid or solid) was surrounded on two sides by the opposite phase. Two-phase MD simulations were started from this initial configuration and allowed to continue for several thousand time steps after either liquid or solid state was reached [usually no more than 10 ps (1 ps = 10^{-12} s)]. In our opinion, a proper determination of the final configuration can be made by examination of the structure and is straightforward because the structures of solid and melt are not similar at high P and T. Atoms in the solid (crystalline) state are arranged with long-range order somewhat distorted by thermal motion. If there is no such long-range order at about the same density, it is either in the amorphous or liquid state. The determination is especially simple if the system freezes into a simple cubic ordered structure. Melting is also quite easy to recognize by comparison of the final configuration with the initial liquid in the computational box. In addition to examining the final configuration, we made animations of each simulation and controlled volume changes, radial distribution function (RDF), and coordination number (CN). These values were calculated as averages over 100, 400, and 2000 time steps; therefore, we also controlled the drift of the averages. In each determination of the phase state of the final state of a simulation, these four criteria (animation, RDF, CN, and volume change) were internally consistent.

Constant pressure MD simulations were performed with the Parinello-Rahman method (Parinello and Rahman 1981). Long-range coulombic interactions were calculated using the method of Ewald (1921). The value of the time step ranged from 1 to 3 fs (1 fs = 10^{-15} s). Because

of the use of a link-cell method (Quentrec and Brot 1975), the cut-off radius could be chosen up to the length of the MD cell side (unlike the minimum-image convention, in which the cut-off cannot be larger than one-half the MD cell side). It is especially useful for analyzing a size effect because if the minimum-image convention is used the cut-off must be rather small (less than one-half the MD cell side) in a system containing a small number of particles. It influences results for small systems, in addition to a pure size effect, and does not allow one to judge the size effect. Equations of motion are integrated using the Refson (1985) modification of the Beeman (1976) algorithm, which in the case of an atomic system is equivalent to the Verlet (1967) algorithm. The choice of the system size used (512 atoms in one-phase and 1024 atoms in two-phase simulations) is justified by a previous study (Matsui 1989) and by our analysis (see Appendix).

In all our simulations velocities were scaled during the equilibration period. Averages were calculated without scaling of velocities, allowing temperature to fluctuate around an average value. Taking into account "statistical inefficiency" (Allen and Tildesley 1987), errors of the temperature calculations are <30 K, reaching a maximum at the highest simulated T (above 7000 K).

RESULTS AND DISCUSSION

One-phase (conventional) simulation

Before starting the two-phase simulations, we checked how well our potentials reproduce properties of NaCl and MgO. To check the applicability of the IP at high P and T, extended MD simulations were performed. For both

TABLE 2. Interaction potential parameters for MgO and NaCl

Atom	q (e)	ρ_i (nm)	r_i (nm)	D_i^* (kcal/mol)	α_i^* (nm^{-1})	R_{i0}^* (nm)	C_i^* (10^6 kcal$^{\frac{1}{2}}$nm^3/mol)
Mg**	1.251	0.01180	0.13211	10.4	10.5	0.064	0.274
O	−1.251	0.015275	0.19797	1.0	7.5	0.135	0.181
Na**	0.966	0.01105	0.13869	8.17	5.5	0.052	0.167
Cl	−0.966	0.02155	0.22150	1.0	4.5	0.168	1.910

* $D_{ij} = D_i + D_j$, $\alpha_{ij} = \alpha_i + \alpha_j$, $R_{ij0} = R_{i0} + R_{j0}$, $C_{ij} = C_i C_j$.
** $D_{MgMg} = D_{NaNa} = 0$.

NaCl and MgO we simulated about 150 PVT points from 300 to 6000 K and from 1 bar to 2000 kbar. The resulting data for the solid (B1) phases were fitted with the high-temperature form of the Birch-Murnaghan equation of state (Birch 1952; Murnaghan 1937; Saxena et al. 1993):

$$P = 3K_T(1 + 2f)^{5/2}(1 + 2\xi f) \qquad (5)$$

where $\xi = \frac{3}{4}(K'_T - 4)$, $f = \frac{1}{2}[(V_{1,T}/V_{P,T})^{\frac{2}{3}} - 1]$, $K'_T = K'_{300} + K'_1(T - 300) \ln(T/300)$, $V_{1,T} = V_0 \exp(\int \alpha\, dT)$, $K_T = 1/\beta_T$, $\beta_T = \beta_0 + \beta_1 T + \beta_2 T^2 + \beta_3 T^3$, and $\alpha = \alpha_0 + \alpha_1 T + \alpha_2 T^{-1} + \alpha_3 T^{-2}$. The calculated parameters for NaCl and MgO are given in Table 3. The unit for thermal expansivity (α) in Equation 5 and Table 3 is inverse kelvins and for compressibility (β), inverse bars. $V_{1,T}$ is volume at 1 bar and temperature, T, in cubic centimeters per mole, V_0 is volume at ambient temperature and pressure. Equation 5 gives very reasonable fits for both NaCl and MgO. The maximum error in pressure is <1%.

Figures 1 and 2 show a comparison of our simulated and experimental data for NaCl. The simulated 300 K isotherm (Fig. 1) is in good agreement with the experimental data on volume change at 300 K (Heinz and Jeanloz 1984; Liu and Bassett 1973; Sato-Sorensen 1983) and pressures of more than 600 kbar. At 600 kbar, the volume of NaCl is approximately one-half the value at normal pressure. P-V experimental data for the B1 phase (Decker 1971; Liu and Bassett 1973; Sato-Sorensen 1983) are internally consistent. P-V data for the B2 phase are rather controversial. As one can see (Fig. 1), there is a rather large difference between the measurements of Sato-Sorensen (1983) and Heinz and Jeanloz (1984). Theoretical predictions of the pressure of the B1-B2 transition are also rather controversial, ranging from 60 kbar (Murti and Salvarajan 1980) to 270 kbar (Froyen and Cohen 1984). We found the B1-B2 transition pressure for NaCl at 380 kbar and 300 K. Taking into account the large scatter of theoretical and experimental pressures [230–330 kbar (Fritz et al. 1971; Liu and Bassett 1973; Sato-Sorensen 1983)] for the transition, we consider our prediction to be in rather good agreement with the experimental data. Therefore, we conclude that our interatomic potential works well when pressure is probing shorter than normal distances (up to 600 kbar) between Na and Cl atoms. It is also suitable for describing interactions where the coordination changes (B1-B2 transition). Let us consider how the IP works at elevated temperatures. Figure 2 shows calculated isotherms compared with experimental isotherms (Boehler and Kennedy 1980) that were measured up to 32 kbar and 773 K. The comparison shows almost quantitative agreement.

For calculation of MgO properties, we thoroughly checked other pairwise potentials. We calculated the 300 K isotherm using a pairwise IP developed earlier (Allan et al. 1991; Leinenweber and Navrotsky 1988; Matsui 1989) and compared the results with experimental data, other predictions, and the isotherm calculated using the IP of this study (Eq. 5). Figure 3 shows the result of the comparison (some of the predictions are not shown in the

TABLE 3. Values of coefficients in Equation 5

Parameter	MgO (B1)	NaCl (B1)
V_0	11.312	26.333
$\alpha_0 \times 10^6$	2.058	38.503
$\alpha_1 \times 10^9$	1.530	8.214
$\alpha_2 \times 10^3$	24.558	9.983
α_3	−4.573	0.712
$\beta_0 \times 10^7$	5.453	34.713
$\beta_1 \times 10^{11}$	12.527	34.493
$\beta_2 \times 10^{14}$	−2.686	120.157
$\beta_3 \times 10^{17}$	1.087	21.476
K'_{300}	4.642	4.737
$K'_1 \times 10^4$	0.050	0.233

figure; see the figure caption). It is clear that our IP gives better results than any of the other pairwise potentials. Matsui's (1989) IP is of about the same quality as ours and could be used. However, we wanted to use the identical form of the IP for both NaCl and MgO (Matsui used the Buckingham potential) calculated by the same method. Potential-induced breathing (PIB) models (Mehl et al. 1986, 1988) give worse results. A recent PIB model (Isaak et al. 1990) predicts a very reasonable 300 K isotherm, as does the variationally stabilized, modified electron-gas model (Wolf and Bukowinski 1988). Our values of K_T and K'_T are 172.2 GPa and 4.64, respectively. These compare very well with the data by Isaak et al. (1990), who obtained $K_T = 180.1$ GPa with $K'_T = 4.15$. Corresponding experimental values (Chang and Barsch 1969; Sumino et al. 1983) are 160.5 GPa and 4.22. We also simulated the B1-B2 transition of MgO and found that, at 300 K, the B1 phase is less stable than the B2 phase at pressures above 5500 kbar. Mehl et al. (1988) found the pressure of the B1-B2 transition for MgO to be 5150 kbar. We compared the simulated thermal expansion (Eq. 5) with the thermal expansion data of Saxena et al. (1993) by calculating a few isotherms up to 3000 K (Fig. 4). The 300 K isotherm fitted to experimental data by Mao and Bell (1979) is also shown for comparison. Saxena et al. (1993) assessed a large body of experimental data on PVT properties of minerals and mineral equilibria involving periclase. Their equation of state derived from the experimental data can be considered as a weighted average. As one can see, the agreement is reasonable (Fig. 4). The difference between the MD simulated volumes and those calculated by Saxena et al. (1993) becomes rather large above 600 kbar and 1000 K. Duffy et al. (1995) measured the 300 K isotherm for MgO up to 227 GPa. This isotherm is consistent with our equation of state within experimental uncertainties.

The probable explanations of the predictive power of our IP are as follows: (1) We fitted various properties that require that the energy and its first, second, and third derivatives be correctly reproduced. This allows rather precise extrapolation of the potential function to the range of interatomic distances not represented at ambient conditions. (2) Parameters were calculated without assuming the symmetry of NaCl and MgO. (3) The particular form
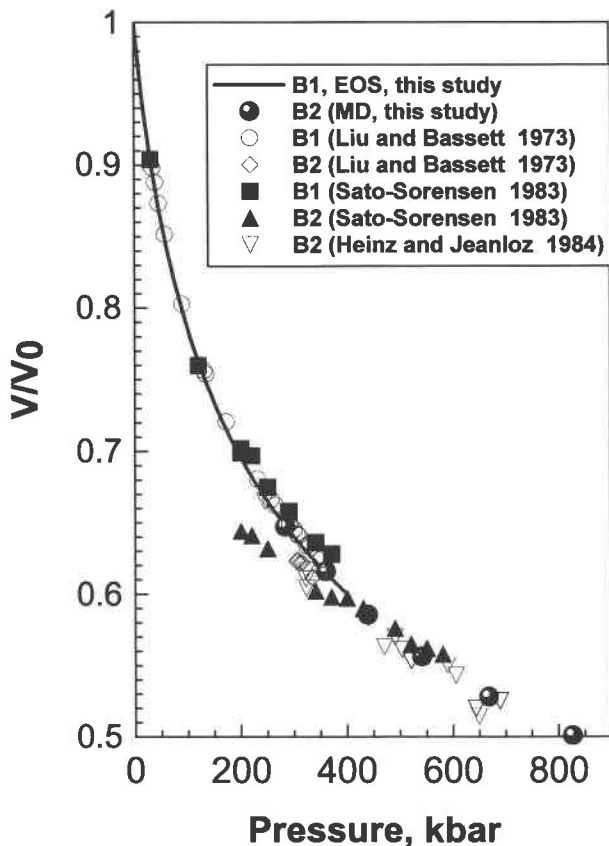
FIGURE 1. Pressure dependence of the volume of NaCl at 300 K for the B1 and B2 phases, in comparison with the experimental data. Solid line represents a fit to the MD-simulated data for the B1 phase (Eq. 5 with parameters from Table 3). Shaded spheres indicate volumes of the B2 phase.
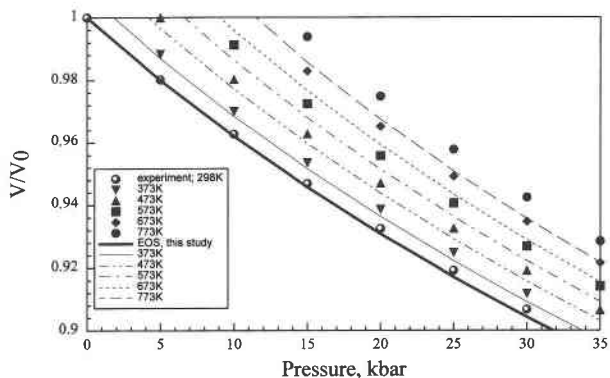

FIGURE 2. Volume of NaCl (B1) calculated using Equation 5 at six temperatures (shown by continuous curves) in comparison with experimental data of Boehler and Kennedy (1980).

of the IP was compared with other forms (Urusov and Dubrovinsky 1989) and found to be superior.

In summary, our potentials work well over a wide range of P and T conditions and have the same or better predictive capability than other potentials.

Two-phase simulation of melting transition

The computational box was prepared as described before. Figures 5–8 provide insight into the typical procedure for determination of temperature brackets at a given pressure. These figures illustrate, in particular, the determination of T_m at 1400 kbar. The temperature brackets were located at 6700 K (solid more stable than liquid) and 7100 K (liquid more stable than solid). Actually, the determination of a temperature interval at a given pressure is equivalent to the determination of a pressure interval at a given temperature; the essential part is that the determined brackets should be close enough to define the melting curve with sufficient precision.

Figure 5 shows two typical MD simulation experiments. Both consist of 12 images of atomic configurations taken at different stages of the simulation. Figures 5a–5c

show crystallization and Figures 5d–5f show melting. The kinetics of both processes are rather fast; a two-phase initial system becomes homogeneous within 4000 time steps (4.8 ps). This is in agreement with Lee and Kubicki (1993), who observed nucleation in MgO melt within 3 ps. Note that in accordance with experimental observations [Phillpot et al. (1989) and references therein] both crystallization and melting are initiated at the interface.

Figure 6 shows a typical dependence of the volume of an initially two-phase system. At a temperature above T_m the volume steadily increases because the melting front advances into the crystal (solid) portion of the two-phase system. In contrast, volume decreases at lower temperature.

The determination of the phase in the resulting configuration is made by analysis of the radial distribution function (RDF) $g_{ij}(R)$ (Fig. 7), which is calculated as a probability density to find an atom of kind j at the distance R from an atom of kind i. The RDF is calculated as an average over atoms i and time. Figure 7 shows the RDF $g_{Mg-O}(R)$ calculated between time steps 6000 and 8000 at 6700 and 7100 K and 1400 kbar. These RDFs show quite distinct behavior. One of them (at 7100 K) is typical of liquid structure. The RDF calculated at 6700 K exhibits clear splitting of the second peak into two peaks and the appearance of a fourth peak, which is higher than the second; this is typical of the cubic structure.

Figure 8 shows the running coordination number (CN) calculated at the same conditions as the RDFs above. CN of Mg is about 6 in both the solid and the liquid. This is typical at high pressure at temperatures close to melting. However, the behavior of CN as a function of distance is rather different. There is a clear flattening of $CN(R)$ at 6700 K, which is indicative of crystal structure. If a cubic crystal were not distorted by thermal motion it would have completely flat $CN(R)$ at R values between the first and second coordination spheres.

One might get the impression that we guessed the temperatures 6700 and 7100 K at a pressure of 1400 kbar; this is not the case. First we simulated MgO at 8000 K
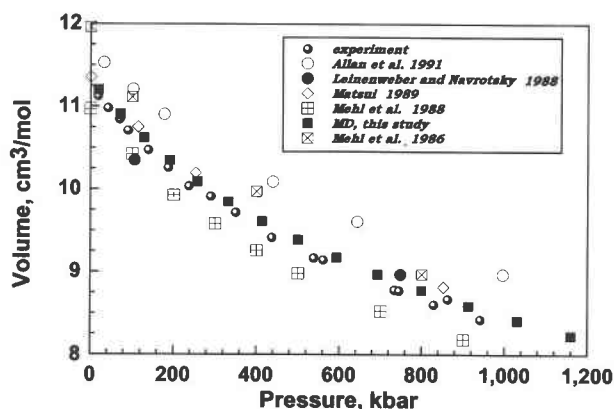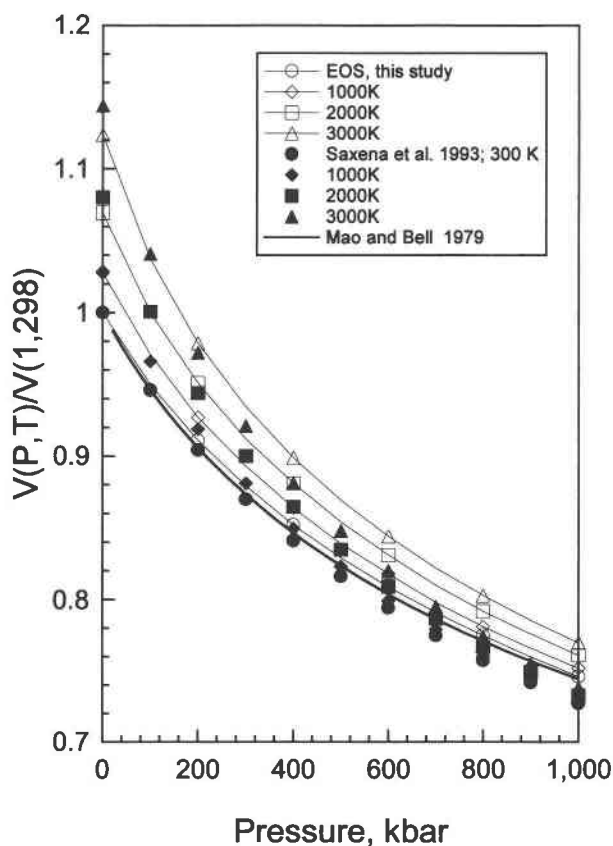
FIGURE 3. Calculated volumes of MgO at 300 K as a function of pressure in comparison with experimental data from Perez-Albuerne and Drickamer (1965) and Mao and Bell (1979). The experimental data are shown by shaded spheres. Solid squares show the MD-simulated results using the IP given by Equation 4 with parameters given in Table 2. The results of our MD calculations using previously developed IPs by Allan et al. (1991), Leinenweber and Navrotsky (1988), and Matsui (1989) are shown by open circles, solid circles, and diamonds, respectively. Squares indicate the results of Mehl et al. (1986) and Mehl et al. (1988), which were obtained by using the potential-induced breathing (PIB) model. Results of Mehl et al. (1986) are shown with the thermal correction according to Wolf and Bukowinski (1988).

FIGURE 4. Comparison of MgO volumes (Saxena et al. 1993; shown by solid symbols) with those calculated using Equation 5 (Eq. 5 is fitted to MD-calculated MgO volumes, shown by open symbols). The 300 K isotherm by Mao and Bell (1979) is shown as a curve without symbols. Saxena et al. (1993) fitted the available experimental data on thermoelastic properties and phase equilibria involving periclase using an equation of state in the form of Equation 5.

and found that it was liquid. Next we simulated MgO at 5000 K and found that it was solid. In subsequent simulations, MgO was solid at 6500 K but liquid at 7250 K. Proceeding in this manner, we finally found the temperature brackets 6700 and 7100 K. In principle, it is possible to find T_m with smaller brackets; however, we think that the current precision at such a high pressure is sufficient. From such temperature (or pressure) brackets, we determined the melting curves for NaCl and MgO.

NaCl and MgO melting curves

Melting of NaCl was experimentally studied by Akella et al. (1969). The room pressure T_m value was found to be 1073.8 K. T_m increases with increasing pressure, and at 65 kbar (the highest experimental pressure reached) it is 1829 K.

Figure 9 compares the calculated pressure dependence of the melting transition of NaCl with the experimental data. The difference between the simulated and experimental melting curves is <100 K at any pressure. The room pressure T_m value is between 1100 and 1150 K. The melting curve flattens at pressures above 300 kbar, near the triple point (B1 + B2 + melt), which we did not locate exactly. At pressures higher than 300 kbar, we performed two-phase simulations with the B1 or B2 structure as the solid part of the computational box. Open triangles in Figure 9 indicate stability of the B2 phase. It is interesting that at 3000 K and 600 kbar the final product of the simulation is melt if the initial solid had the B1 structure and the final product is solid (B2) if the

initial solid had the B2 structure. At pressures higher than 400 kbar the melting curve has a higher slope because of the B1-B2 transition.

The MgO melting curve is easier to calculate because it is not complicated by the B1-B2 transformation at any pressure corresponding to the Earth's interior. Using the same procedure used in the simulation of the NaCl(B1)-melt transition, we calculated the melting P-T curve for periclase (Fig. 10). The experimental T_m value at 1 bar (Kracek and Clark 1966) is 3098 K. The simulated T_m is almost the same. With our procedure, we do not know the exact melting temperature but simply that at 1 bar and 3100 K the two-phase system freezes and at 3250 K it melts. Ohtani (1983) predicted a pressure dependence of T_m for MgO; it is schematically shown in Figure 10. The melting curves of Ohtani and the present study are very similar up to 250 kbar. Above 250 kbar, Ohtani's curve lies at higher pressures than ours. This is probably because Ohtani, using the empirical equation of Kraut and Kennedy (1966), extrapolated experimental data well
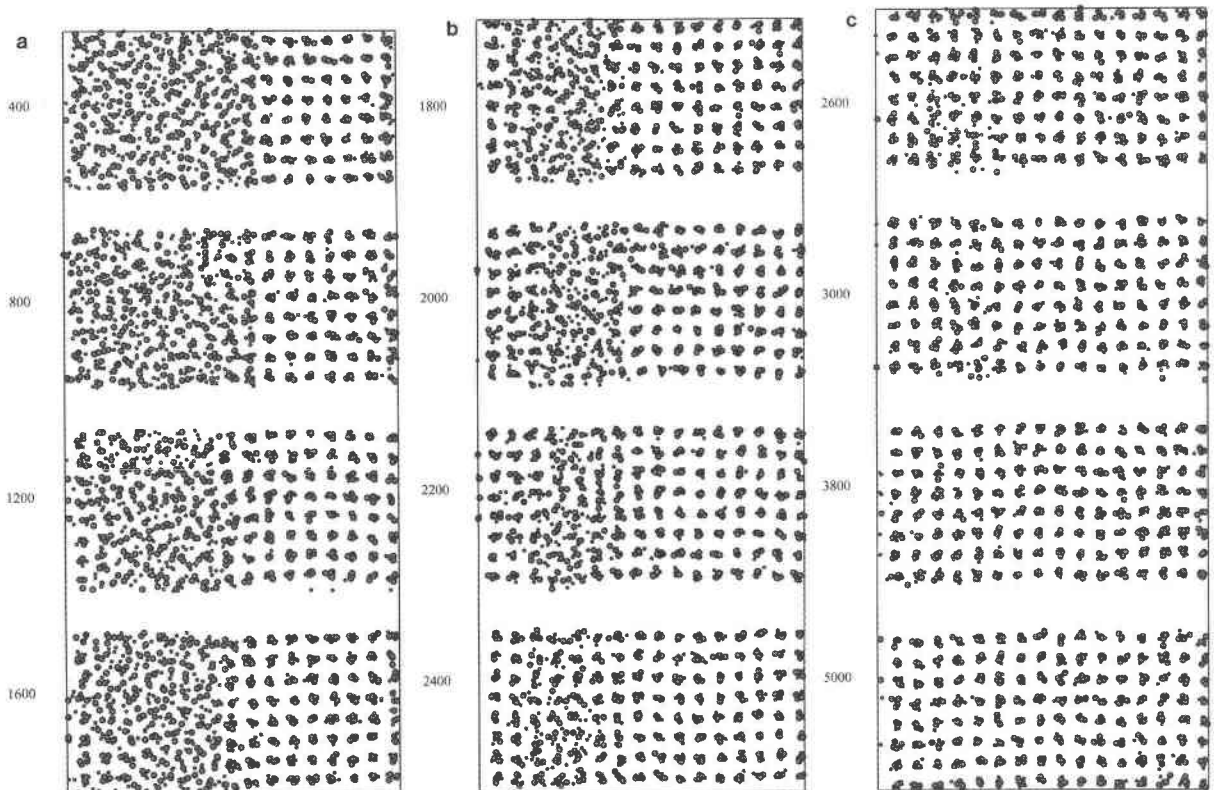
FIGURE 5. Simulation of the time evolution of the two-phase MgO system at 1400 kbar and 6700 K (**a–c**) and 7100 K (**d–f**). A frontal view of the system is shown. The liquid part of the system is on the left side and the solid part is on the right at the beginning of the simulations. Each part consists of 512 atoms; overall size of the system is 1024 atoms. Numbers on the left indicate the time step at which the snapshot is taken (each time step is 1.2 fs for both simulations). O atoms are represented by larger circles; Mg is shown by smaller circles. Parts **a–c** show how a crystallization front progrades into the liquid from both sides of the computational cell owing to the three-dimensional periodic boundary conditions. The front propagates in the direction perpendicular to the interface; crystallization clearly occurs at the surface (not unexpectedly). The last picture of the configuration of atoms in **c** (time step 5000) shows a highly defective cubic crystal. Further simulation (not shown) reduces the defects. Parts **d–f** show the development of the same system into the liquid structure (see also Figs. 6–8) at higher temperature, providing an atomistic picture of the melting process. Again, melting begins at the contact of the liquid and solid parts (time step 1200, **d**). At time step 2800, two layers of atoms can still be seen preserving long-range ordering in the direction parallel to the interface. At time step 3200, the traces of crystal structure are still visible. They gradually disappear, and further equilibration of an already homogeneous system gives a picture typical of a liquid structure (the coordination number and the radial distribution function were calculated during 4000 time steps beginning at the 4000 time step; they are shown in Figs. 7 and 8).

beyond the P-T range of existing data. Note that Ohtani (1983) predicted (though somewhat overestimated) the melting curve of $MgSiO_3$ perovskite, which is in reasonable agreement with the experimental data of Zerr and Boehler (1993a, 1993b) and with the two-phase MD simulation of $MgSiO_3$ perovskite melting (Belonoshko 1994). Jackson's (1977) prediction based on the similarity of the MgO-SiO_2 and LiF-MgF_2 phase diagrams is very close to Ohtani's and ours.

Zerr and Boehler (1994) recently published melting temperatures of MgO for pressures up to 315 kbar. The melting temperature at this pressure is about 4000 K, which is considerably lower than all predictions. The initial slope of their melting curve is very low compared to previously published estimates (Jackson 1977; Ohtani 1983; Cohen and Gong 1994). Taking into consideration the internal inconsistency among results obtained using diamond-anvil cells (DAC) with laser heating [e.g., on wüstite melting (Boehler 1992; Knittle and Jeanloz 1991; Shen et al. 1993)] as well as the inconsistency between the results of shockwave and DAC measurements of Fe melting (the differences in both cases are more than 1000 K), we believe that the difference between our results and those of Zerr and Boehler can be accounted for in future work.

Cohen and Gong (1994) (hereafter, CG) predicted that MgO melting curves lie at significantly higher temperatures than those determined by others. Unfortunately, CG did not use their procedure of calculating melting curves for any compound other than MgO. Our simulation for
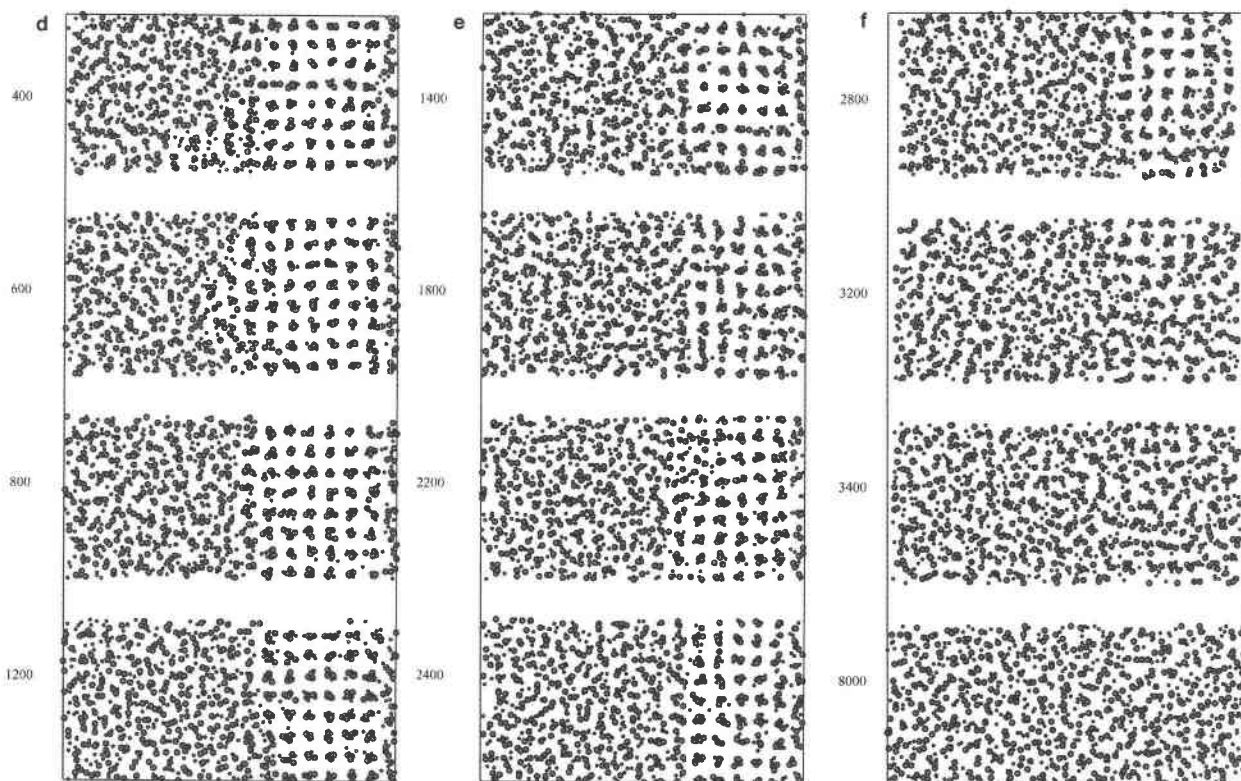
FIGURE 5.—Continued

NaCl demonstrates that our procedure should be valid for MgO. Comparison of their predictions with Zerr and Boehler's (1994) data suggests that the procedure used by CG may not be entirely satisfactory.

Here we compare in more detail our results with those obtained by CG. Both studies used molecular dynamics, but interatomic potentials were calculated in very different ways. CG used a PIB model, whereas we used a two-body central-force IP (Eq. 4). However, both IP models predict similar properties for MgO, including equations of state in good agreement with experiment. Moreover, both potentials predict the B1-B2 MgO phase transition at about the same pressure. Because PVT properties are directly related to the energy change, this means that the energy surface is also reproduced by both methods (the energies might be different, but the energy difference must be constant). Therefore, the difference in T_m values probably cannot be explained by differences between interatomic potentials.

Cohen and Gong actually performed two kinds of simulations: One set of simulations of clusters in free space (zero pressure) and another set of simulations in a cubic box with perfectly elastic walls. CG determined T_m for clusters with 64, 216, 512, and 1000 atoms and then extrapolated the temperature-size dependence to an infinite size, or the bulk system. MD simulations in free space are known to exhibit high hysteresis (± 500 K), which prevents us from judging how well the experimental value
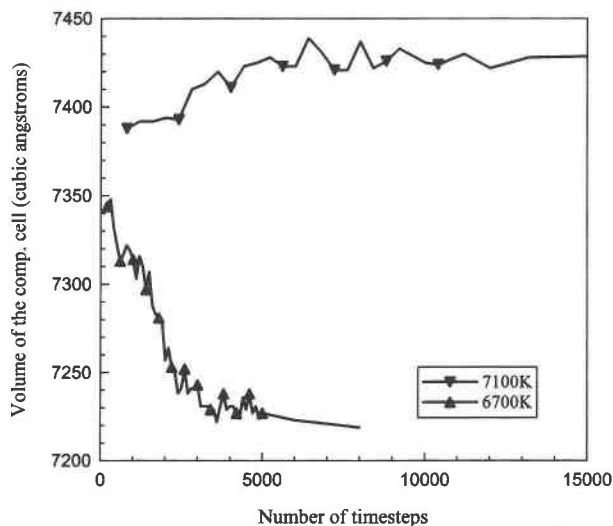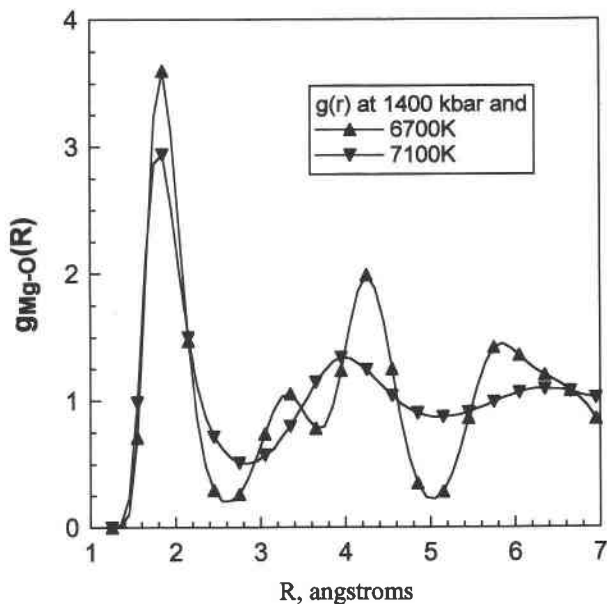

FIGURE 6. The volume dependence of a two-phase system at 1400 kbar at two temperatures. Snapshots of the system are presented in Figure 5. The initial volume (time step zero) is the same at both temperatures (7900 Å³). A solid line connects points indicating values of the volume averaged over 100 (at 6700 K) and 400 (at 7100 K) time steps.

FIGURE 7. Radial distribution functions (RDF) of O around Mg calculated at 1400 kbar and 6700 and 7100 K. The RDF is calculated as the density of O atoms at the distance R from Mg divided by a uniform density of O atoms. Both RDFs were calculated by averaging over 4000 time steps between 4000 and 8000 time steps (each time step is 1.2 fs). The RDF at 7100 K is typical of those of the liquid structure. The RDF at 6700 K shows distinct solidlike behavior. The splitting of a second peak into two and the appearance of a fourth peak at 6 Å are characteristic of the cubic crystal structure. The RDF at 6700 K is very similar to the RDF given by Lee and Kubicki (1993) (see their Fig. 2) for "defective" periclase in their simulation of MgO crystallization.
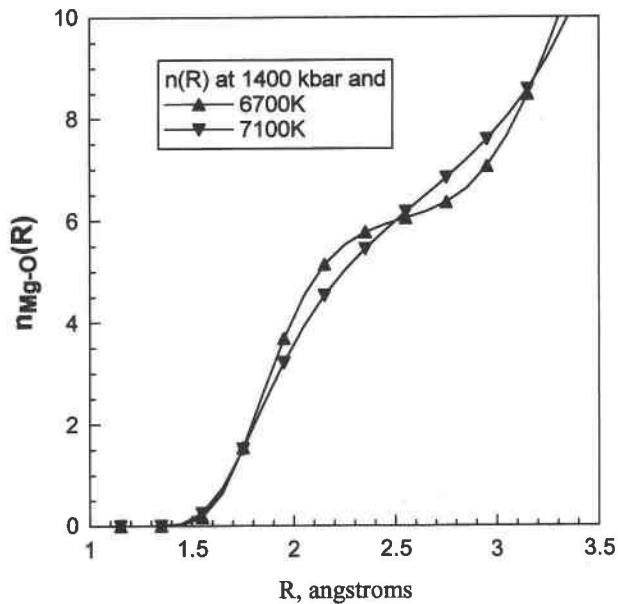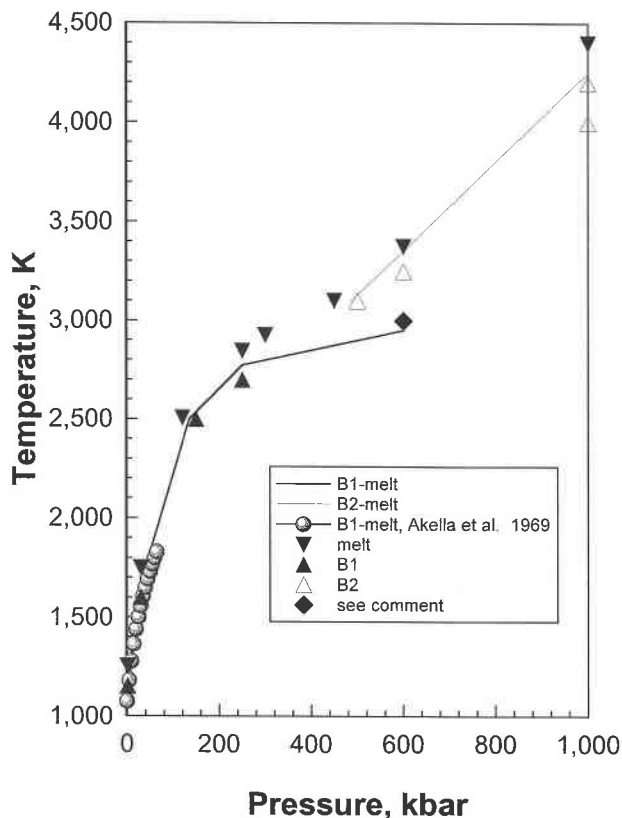

FIGURE 8. Running coordination number (CN) calculated for the same conditions as in Figure 7. CN is calculated as a volume integral of the RDF. The figure demonstrates that the solid and the liquid have CN values close to 6. This is in agreement with Cohen and Gong's (1994) simulation. CN at lower temperature has a distinct step between the first and second coordination spheres (at approximately 2.5 Å; compare with RDF in Fig. 7).

of T_m at 1 bar pressure is reproduced. T_m calculated by CG at 1 bar is between 2700 and 3700 K, a 1000 K interval. CG noted the high hysteresis at 1 bar; this hysteresis decreases with increasing pressure.

CG made another set of simulations by placing Mg and O atoms in a cubic box. This cubic box changes the properties of the system. It is well known that the pressure within a liquid (melt) exhibits oscillating behavior as a function of distance between the confining walls if the distance between walls is comparable to the size of the molecules (cf. Christensen et al. 1987, Henderson and van Swol 1988, Belonoshko and Shmulovich 1987, and references therein). Pressure in a confined liquid can be greater or smaller than that in a corresponding bulk liquid of the same density, depending on the distance between the walls (L). This effect becomes less pronounced when L increases; however, the fluid is influenced by the walls up to at least ten atomic sizes. Of course, the magnitude of the effect depends on the detailed interactions between atoms and between the atoms and the walls, as well as on the exact geometry of the pores (slitlike, spherical, cylindrical, cubic, etc.). The interatomic potential for Mg or O with the wall becomes infinite when the distance of

separation is less than a critical value. In the particular case addressed by Cohen and Gong one might expect strong interactions between the walls and the MgO cluster because of the size of the simulated clusters (64, 216, 512, and 1000), which compose 4, 6, 8, and 10 layers of atoms within the box. In all cases, the integer number of layers corresponds to minima on the periodic pressure-size curve. A simulation using a cluster of intermediate size would reveal the effect of the periodicity. An extrapolation improves the situation slightly, because the amplitude of the pressure oscillation indeed decreases as the size of the cluster increases. However, even the largest cluster (1000 atoms or 10 layers) is still within the size for which a pronounced wall influence is expected (Christensen et al. 1987). (Note that CG's 1000 atoms and our 1024 atoms are not comparable; we used three-dimensional periodic boundary conditions to simulate bulk behavior.) CG observed a linear dependence of T_m on $1/R$, where R = size of the system. By our explanation this simply means that the amplitude of the pressure oscillations decreases as $1/R$ with the system size. The slope of the T_m dependence with $1/R$ increases with increasing pressure because the period of the pressure oscillations becomes smaller (high pressure forces monolayers to come closer to each other). Therefore, we believe that CG observed the same melting temperatures but at pressures lower than those in the bulk. More recently, Cohen and Kluge (1995) obtained a melting curve of MgO using a
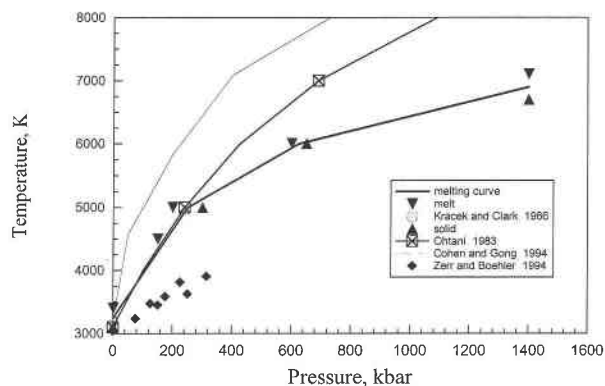
FIGURE 10. A phase diagram of MgO melting. The triangles indicate stability of the simulated solid phase; inverted triangles indicate stability of the melt. Stability was determined by two-phase simulations as explained in the text. A typical procedure is illustrated in Figures 5–9. Not all simulated data are shown but only the *P-T* points closest to the position of the melting transformation. In addition, one point at 150 kbar and 4500 K is shown indicating that at this condition melt was found to be more stable than periclase. The resulting continuous melting curve is shown schematically for visual convenience. The room pressure melting temperature indicated by the filled sphere is from Kracek and Clark (1966). The experimental data of Zerr and Boehler (1994) are shown by solid diamonds.

FIGURE 9. Phase diagram for melting of the B1 and B2 phases of NaCl. Triangles indicate stability of the simulated solid phase; inverted triangles indicate stability of the melt. Stability was determined by two-phase simulations as explained in the text. A typical procedure is illustrated in Figures 5–9. Not all simulated data are shown but only the *P-T* points closest to the position of melting transformation. The resulting continuous melting curve is shown schematically for convenience to guide the reader's eye. Open triangles indicate stability of the B2 phase. The solid thick curve with solid spheres is experimental data of Akella et al. (1969). Solid diamond at 3000 K and 600 kbar either indicates the conditions of crystallization of the B2 structure when the solid part of the two-phase system was B2, or indicates the melt if the solid part of two-phase system was B1. In other words, at these conditions melt is more stable than B1 and less stable than B2 phase. Therefore, we drew a continuous line to schematically indicate the B1-melt transition below that point (3000 K and 600 kbar).

64-atom system with periodic boundary conditions. They concluded that "the calculated slope of the melting curve was somewhat less" than that obtained by Cohen and Gong (1994).

REFERENCES CITED

Agee, C.B. (1993) Introduction to the special section on magma ocean. Journal of Geophysical Research, 98, 5317.

Agee, C.B., and Longhi, J., Eds. (1992) Physics and chemistry of magma oceans from 1 bar to 4 Mbar. LPI Technical Report, 92-03, 79 p.

Akella, J., Vaidya, S.N., and Kennedy, G.C. (1969) Melting of sodium chloride at pressures to 65 kbar. Physics Review, 185, 1135–1140.

Allan, N.L., Braithwaite, M., Cooper, D.L., Mackrodt, W.C., and Wrigh, S.C. (1991) Ionic solids at high pressures and elevated temperatures: MgO (periclase). Journal of Chemical Physics, 95, 6792–6799.

Allen, M.P., and Tildesley, D.J. (1987) Computer simulation of liquids, 385 p. Clarendon, Oxford, U.K.

Anastasiou, N., and Fincham, D. (1982) Programs for the dynamic simulation of liquids and solids: II. MDIONS: Rigid ions using the Ewald sum. Computer Physics Communications, 25, 159–172.

Anderson, D.L. (1989) Theory of the Earth, 366 p. Blackwell Scientific, Boston.

Animalu, A.O.E. (1977) Intermediate quantum theory of crystalline solids, 574 p. Prentice-Hall, Englewood Cliffs, New Jersey.

Bartels, R.A., and Schuele, D.E. (1965) Pressure derivatives of the elastic constants of NaCl and KCl at 295 K and 195 K. Journal of Physics and Chemistry of Solids, 26, 537–549.

Beeman, D. (1976) Some multistep methods for use in molecular dynamics calculations. Journal of Computational Physics, 20, 130–139.

Belonoshko, A.B. (1994) Molecular dynamics of $MgSiO_3$ perovskite at high pressures: Equation of state, structure and melting transition. Geochimica et Cosmochimica Acta, 58, 4039–4047.

Belonoshko, A.B., and Shmulovich, K.I. (1987) A molecular-dynamics study of a dense fluid in micropores. Geochemistry International, 24, 1–12 (translated from Geokhimiya, 11, 1523–1534, 1986).

Birch, F. (1952) Elasticity and constitution of the Earth's interior. Journal of Geophysical Research, 57, 227–286.

—— (1986) Equation of state and thermodynamic parameters of NaCl to 300 kbar in the high-temperature domain. Journal of Geophysical Research, 91, 4949–4954.

Boehler, R. (1992) Melting of the Fe-FeO and Fe-FeS systems at high pressure: Constraints on core temperatures. Earth and Planetary Science Letters, 111, 217–227.

—— (1993) Temperature in the Earth's core from melting-point measurements of iron at high static pressures. Nature, 363, 534–536.

Boehler, R., and Kennedy, G. (1980) Equation of state of sodium chlorite up to 32 kbar and 500°C. Physics and Chemistry of Solids, 41, 517–523.

Born, M., and Huang, K. (1954) Dynamical theory of crystal lattices, 420 p. Oxford University Press, New York.

Catlow, C.R.A., and Macrodt, W.C., Eds. (1982) Computer simulation of solids. In Lecture Notes in Physics, 166, 320 p.

Chang, Z.P., and Barsch, G.R. (1969) Pressure dependence of the elastic constants of single-crystal magnesium oxide. Journal of Geophysical Research, 74, 3291–3294.

Christensen, H.K., Gruen, D.W.R., Horn, R.G., and Israelachvili, J.N. (1987) Structuring in liquid alkanes between solid surfaces: Force measurements and mean-field theory. Journal of Chemical Physics, 87, 1834–1841.

Cohen, A.J., and Gordon, R.G. (1976) Modified electron-gas study of the stability, elastic properties and high pressure behavior of MgO and CaO crystals. Physics Review B, 14, 4503–4505.

Cohen, R.E., and Gong, Z. (1994) Melting and melt structure of MgO at high pressures. Physical Review B, 50, 12301–12311.

Cohen, R.E., and Kluge, M.D. (1995) Thermodynamics of melting of MgO at high pressures from first principles. V.M. Goldschmidt Conference, Program and Abstracts, 1995, 37.

Decker, D.L. (1971) High-pressure equation of state for NaCl, KCl, and CsCl. Journal of Applied Physics, 42, 3239–3244.

Dekker, A.J. (1965) Solid state physics, 540 p. Macmillan, London, U.K.

Dove, M.T. (1993) Introduction to lattice dynamics, 258 p. Cambridge University Press, Cambridge.

Duffy, T.S., Hemley, R.J., and Mao, H.K. (1995) Equation of state and shear strength at multimegabar pressures: Magnesium oxide to 227 GPa. Physical Review Letters, 74, 1371–1374.

Dziewonski, A.M., and Anderson, D.L. (1981) Preliminary reference Earth model. Physics of the Earth and Planetary Interior, 25, 297–359.

Ewald, P.P. (1921) Die Berechnung optischer und elektrostatischer Gitterpotentiale. Annal Physik, 64, 253–287.

Fritz, J.N., Marsh, S.P., Carter, W.J., and McQueen, R.G. (1971) The Hugoniot equation of state of sodium chloride in the sodium chloride structure. In NBS Special Publication, 326, 201–208.

Froyen, S., and Cohen, M.L. (1984) Structural properties of NaCl. Physical Review B, 29, 3770–3772.

Haile, J.M. (1992) Molecular dynamics simulation: Elementary methods, 489 p. Wiley, New York.

Heinz, D.L., and Jeanloz, R. (1984) Compression of the B2 high-pressure phase of NaCl. Physics Review B, 30, 6045–6050.

—— (1987) Measurement of the melting curve of $Mg_{0.9}Fe_{0.1}SiO_3$ at lower mantle conditions and its geophysical implications. Journal of Geophysical Research, 92, 11437–11444.

Hemley, R.J., and Gordon, R.G. (1985) Theoretical study of solid NaF and NaCl at high pressures and temperatures. Journal of Geophysical Research, 90, 7803–7813.

Henderson, J.R., and van Swol, F. (1988) Grand potential densities of wall-liquid interfaces approaching complete drying. Journal of Chemical Physics, 89, 5010–5014.

Hofer, O.C., and Ferreira, R.J. (1966) Covalent and ionic bond orders: Applications to the alkali halides molecules. Journal of Physical Chemistry, 70, 85–94.

Honeycutt, J.P., and Andersen, H.C. (1984) The effect of periodic boundary conditions on homogeneous nucleation observed in computer simulation. Chemical Physics Letters, 108, 535–538.

Isaak, D.G., Cohen, R.E., and Mehl, M.J. (1990) Calculated elastic and thermal properties of MgO at high pressures and temperatures. Journal of Geophysical Research, 95, 7055–7067.

Jackson, I. (1977) Phase relations in the system LiF-MgF₂ at elevated pressures: Implications for the proposed mixed-oxide zone of the Earth's mantle. Physics of the Earth and Planetary Interior, 14, 86–94.

Jha, B.N. (1993) Thermal properties of NaCl and CsCl crystals under high pressure. Physica B, 192, 253–258.

Kapusta, B., and Guillopé, M. (1993) Molecular dynamics study of the perovskite $MgSiO_3$ at high temperature: Structural, elastic and thermodynamical properties. Physics of the Earth and Planetary Interior, 75, 205–224.

Kieffer, S.W. (1979) Thermodynamics and lattice vibrations of minerals: 1. Mineral heat capacities and their relationships to simple lattice vibrational modes. Reviews in Geophysics and Space Physics, 17, 1–19.

Knittle, E., and Jeanloz, R. (1991) The high-pressure phase diagram of $Fe_{0.94}O$: A possible constituent of the Earth's core. Journal of Geophysical Research, 96, 16169–16180.

Kracek, F.C., and Clark, S.P. (1966) Handbook of physical constants, p. 301–344. Geological Society of America, New York.

Kraut, E.A., and Kennedy, G.C. (1966) New melting law at high pressures. Physical Review, 151, 668–675.

Kubicki, J.D., and Lasaga, A.C. (1992) Ab initio molecular dynamics simulations of melting of forsterite and $MgSiO_3$ perovskite. American Journal of Science, 292, 153–183.

Landau, L.D., and Lifshitz, E.M. (1958) Statistical physics, 484 p. Pergamon, London, U.K.

Lee, W.-J., and Kubicki, J.D. (1993) Molecular dynamics simulations of periclase crystallization. Geophysical Research Letters, 20, 2103–2106.

Leinenweber, K., and Navrotsky, A. (1988) A transferable interatomic potential for crystalline phases in the system $MgO-SiO_2$. Physics and Chemistry of Minerals, 15, 588–596.

Liu, L.G., and Bassett, W.A. (1973) Compression of Ag and phase transformation of NaCl. Journal of Applied Physics, 44, 1475–1479.

Mao, H.K., and Bell, P.M. (1979) Equations of state of MgO and ε Fe under static pressure conditions. Journal of Geophysical Research, 84, 4533–4536.

Matsui, M. (1989) Molecular dynamics study of the structural and thermodynamic properties of MgO crystal with quantum correction. Journal of Chemical Physics, 91, 489–494.

Matsui, M., and Price, G.D. (1991) Simulation of the pre-melting behavior of $MgSiO_3$ perovskite at high pressures and temperatures. Nature, 351, 735–737.

Mehl, M.J., Hemley, R.J., and Boyer, L.L. (1986) Potential-induced breathing model for the elastic moduli and high-pressure behavior of cubic alkaline-earth oxides. Physical Review B, 23, 900–923.

Mehl, M.J., Cohen, R.E., and Krakauer, H. (1988) Linearized augmented plane wave electronic calculations for MgO and CaO. Journal of Geophysical Research, 93, 8009–8022.

Murnaghan, F.D. (1937) Finite deformations of an elastic solid. American Journal of Mathematics, 59, 235–260.

Murti, Y.V.G.S., and Salvarajan, T.V. (1980) FCC→SC phase transition in alkali halides. Solid State Communications, 33, 417–418.

Ohtani, E. (1983) Melting temperature distribution and fractionation in the lower mantle. Physics of the Earth and Planetary Interior, 33, 12–25.

Parinello, M., and Rahman, A. (1981) Polymorphic transitions in single crystals: A new molecular dynamics method. Journal of Applied Physics, 52, 7182–7190.

Parker, S.C., Catlow, C.R.A., and Cormack, A.N. (1984) Structure prediction of silicate minerals using energy-minimization techniques. Acta Crystallographica, B40, 200–208.

Parker, S.C., and Price, G.D. (1989) Computer modelling of phase transitions in minerals. Advances in Solid-State Chemistry, 1, 295–327.

Perez-Albuerne, E.A., and Drickamer, H.G. (1965) Effect of high pressures on the compressibilities of seven crystals having the NaCl or CsCl structure. Journal of Chemical Physics, 43, 1381–1387.

Phillpot, S.R., Lutsko, J.F., Wolf, D., and Yip, S. (1989) Molecular-dynamics study of lattice-defect-nucleated melting in silicon. Physical Review B, 40, 2831–2840.

Press, W.H., Flannery, B.P., Teukolsky, S.A., and Vetterling, W.T. (1992)

Numerical recipes (FORTRAN version), 702 p. Cambridge University Press, Cambridge.

Quentrec, B., and Brot, C. (1975) New methods for searching for neighbours in molecular dynamics computations. Journal of Computational Physics, 13, 430–432.

Refson, K. (1985) Molecular dynamics simulation of solid *n*-butane. Physica, 131B, 256–266.

Sato-Sorensen, Y. (1983) Phase transitions and equations of state for the sodium halides: NaF, NaCl, NaBr, and NaI. Journal of Geophysical Research, 88, 3543–3548.

Saxena, S.K., Chatterjee, N., Fei, Y., and Shen, G. (1993) Thermodynamic data on oxides and silicates, 428 p. Springer-Verlag, Berlin.

Saxena, S.K., Shen, G., and Lazor, P. (1993) Experimental evidence for a new iron phase and implications for Earth's core. Science, 260, 1312–1314.

Shen, G. (1994) Melting of minerals under the Earth's lower mantle conditions. Ph.D. thesis. Uppsala University, Uppsala, Sweden.

Shen, G., Lazor, P., and Saxena, S.K. (1993) Melting of wüstite and iron up to pressures of 600 kbar. Physics and Chemistry of Minerals, 20, 91–96.

Smolander, K.J. (1990) Monte Carlo study of the melting and solidification of copper. Physica Scripta, 42, 485–488.

Solomatov, V.S., and Stevenson, D.J. (1993) Nonfractional crystallization of a terrestrial magma ocean. Journal of Geophysical Research, 98, 5391–5406.

Sumino, Y., Anderson, O.L., and Suzuki, I. (1983) Temperature coefficients of elastic constants of single crystal MgO between 80 and 1300 K. Physics and Chemistry of Minerals, 9, 38–47.

Urusov, V.S. (1975) Energetical crystal chemistry, 333 p. Nauka, Moscow (in Russian).

Urusov, V.S., and Dubrovinsky, L.S. (1985) Theoretical modeling of mineral crystal structures. Vestnik Moskovskogo Universiteta, Geologija, 5, 8–28.

——— (1989) Computer simulation of crystal structures and properties of minerals, 250 p. Moscow University Press, Moscow (in Russian).

Urusov, V.S., Dubrovinsky, L.S., Vasserman, E.A., and Eremin, N.N. (1994) Computer simulation of the structure and elastic properties of rutile-type oxides by the method of minimization of the energy of atomic interactions. Crystallography Reports, 39, 446–456.

Verlet, L. (1967) Computer 'experiments' on classical fluids: I. Thermodynamical properties of Lennard-Jones molecules. Physical Review, 165, 201–214.

Wolf, G.H., and Bukowinski, M.S.T. (1988) Variational stabilization of the ionic charge densities in electron-gas theory of crystals: Applications to MgO and CaO. Physics and Chemistry of Minerals, 15, 209–220.

Yoo, C.S., Holmes, N.C., Ross, M., Webb, D.J., and Pike, C. (1993) Shock temperatures and melting of iron at Earth core conditions. Physical Review Letters, 70, 3931–3934.

Zerr, A., and Boehler, R. (1993a) Melting of (Mg,Fe)SiO$_3$-perovskite under hydrostatic, inert conditions to 580 kbar. 1993 Spring Eos Abstract Supplement, p. 168–169.

——— (1993b) Melting of (Mg,Fe)SiO$_3$-perovskite to 625 kilobars: Indication of a high melting temperature in the lower mantle. Science, 262, 553–555.

——— (1994) Constraints on the melting temperature of the lower mantle from high-pressure experiments on MgO and magnesiowustite. Nature, 371, 506–508.

Zoubolis, E.S., and Grimsditch, M. (1991) Refractive index and elastic properties of MgO up to 1900 K. Journal of Geophysical Research, B96, 4167–4170.

APPENDIX: INFLUENCE OF SYSTEM SIZE ON RESULTS

The results of two- and one-phase simulations may be influenced by the number of particles involved in the simulation. Honeycutt and Andersen (1984) noticed that

periodic boundary conditions affect the rate of liquid nucleation. We simulated the two-phase MgO system with 64, 216, and 512 atoms in each of the liquid and solid parts and found their corresponding melting *P-T* conditions at 6000 K. The system with 64 atoms in each part melts at 781.75 ± 6.75 kbar. Systems consisting of 216 and 512 atoms melt at the same pressure (625 kbar) within the precision of our calculated brackets (±25 kbar). The temperatures of solidification and melting at 1400 kbar of the system consisting of 2 × 64 atoms were calculated as 6500 and 7000 K, respectively (the system with 2 × 512 atoms melts at 7100 K and freezes at 6700 K at the same pressure). Therefore, the effect of system size on results rapidly diminishes as the number of atoms increases and is not that great in general. Let us consider how the simulated melting temperature and the properties of a solid might depend on system size.

The difference between the calculated melting temperatures of "small" and "big" systems might be explained by different values of vibrational energies of the solid parts of the computational cells. The energy of the liquid part also might be changed by imposed periodic boundary conditions, especially if the *P-T* conditions are near a phase transformation (Allen and Tildesley 1987). However, the effect of periodic boundary conditions on the properties of the liquid and solid is certainly quantitatively different.

If we simulate a crystal with periodic boundary conditions, then we suppress oscillations with wavelengths larger than the size of the computational cell. Hence, a portion of the low-frequency oscillations cannot be accounted for. According to the Debye model (Born and Huang 1954; Kieffer 1979) for an infinite crystal, we have

$$F_b^{vib} = \frac{9nkT}{\omega_D^3} \int_0^{\omega_D} \ln\left[1 - \exp\left(-\frac{\hbar\omega}{kT}\right)\right]\omega^2 \, d\omega \quad (A1)$$

where k = Boltzmann's constant, $\hbar$ = Planck's constant, n = number of atoms in the formula unit, T = temperature, ω_D = Debye frequency, and F_b^{vib} = energy of oscillation without energy of zero oscillations.

If the lowest possible frequency is ω_s, then Equation A1 should be rewritten as

$$F_s^{vib} = \frac{9nkT}{\omega_D^3 - \omega_s^3} \int_{\omega_s}^{\omega_D} \ln\left[1 - \exp\left(-\frac{\hbar\omega}{kT}\right)\right]\omega^2 \, d\omega. \quad (A2)$$

Assigning $\theta_D = \hbar\omega_D/k$, $\theta_s = \hbar\omega_s/k$, and assuming that $T \ll \theta_D$ (but not $T \ll \theta_s$!), for "big" and "small" systems we have, respectively,

$$F_b^{vib} = -\frac{\pi^4 nkT^4}{5\theta_D^3} \quad (A3)$$

and

$$F_s^{vib} = \frac{\pi^4 nkT^4}{5(\theta_D^3 - \theta_s^3)} + \frac{3nkT^4}{(\theta_D^3 - \theta_s^3)} \int_0^{\theta_s/T} \frac{(\theta/T)^3 \, d(\theta/T)}{\exp(\theta/T) - 1}. \quad (A4)$$

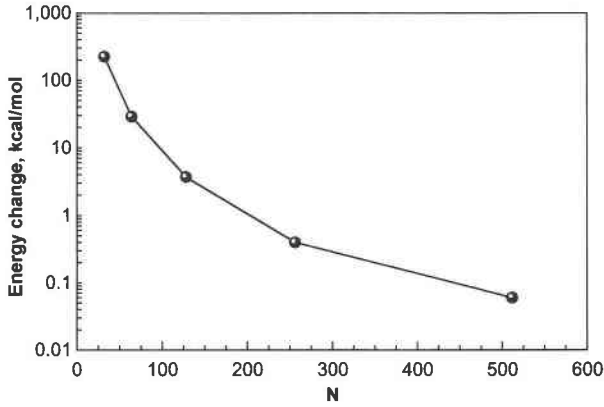From comparison of Equations A3 and A4 it follows that,

APPENDIX FIGURE 1. Difference between vibrational energies of finite and infinite MgO crystals, calculated with the program EMIN as a function of N, number of atoms, at 6000 K and 600 kbar. Quantitatively, this difference is the same at any pressure and at any temperature above the Debye temperature (see text).

depending on the value of θ_s, both situations $-F_b^{vib} > F_s^{vib}$ and $F_b^{vib} < F_s^{vib}$ are possible. However, if $T \gg \theta_D$, then for "big" and "small" systems (F_b^{vib} and F_s^{vib}) we have, respectively,

$$F_b^{vib} = 3nkT \ln\left(\frac{\hbar\omega_D}{kT}\right) - nkT \qquad (A5)$$

and

$$F_s^{vib} = \frac{3nkT}{\omega_D^3 - \omega_s^3}\left[\omega_D^3\ln\left(\frac{\hbar\omega_D}{kT}\right) - \omega_s^3\ln\left(\frac{\hbar\omega_s}{kT}\right)\right] - nkT. \qquad (A6)$$

Therefore, for any physically possible values of ω_D and ω_s, $F_b^{vib} < F_s^{vib}$.

We calculated F^{vib} of MgO and found that the difference between energies for systems with 64 and 512 atoms equals 29.52 kcal/mol at 6000 K and 600 kbar. The MD-simulated melting pressures are 781.75 ± 6.75 and 625 ± 25 kbar at 6000 K for systems with 64 and 512 atoms, respectively, in the "solid" part of the computational box. The calculated energy difference is comparable to the energy corresponding to the pressure shift (volume of MgO at 6000 K and 600 kbar is about 10 cm^3/mol). However, if the liquid part of the box is subjected to the same change owing to the applied periodic boundary conditions, the resulting difference between the vibrational energies cannot explain the observed pressure shift of melting.

Note that according to our calculations the difference between the vibrational energy terms of infinite and finite crystals decreases in proportion to the number of molecules raised to the third power (Appx. Fig. 1). Therefore, the precision of the calculations of the crystal properties depends mainly on the quality of the IP and not on the number of molecules (provided, of course, the number of molecules is more than a few hundred).